*J Mater Sci* (2018) 53:9131–9137

Electronic materials

# Enhanced metal–insulator transition in $V_2O_3$ by thermal quenching after growth

J. Trastoy[1,2,*], Y. Kalcheim[1], J. del Valle[1], I. Valmianski[1], and Ivan K. Schuller[1]

[1] Department of Physics and Center for Advanced Nanoscience, University of California San Diego, La Jolla, CA 92093, USA
[2] Present address: Unité Mixte de Physique, CNRS, Thales, Université Paris-Sud, Université Paris Saclay, 91767 Palaiseau, France

**Received:** 1 December 2017
**Accepted:** 8 March 2018
**Published online:** 15 March 2018



## ABSTRACT

The properties of oxides are critically controlled by the oxygen stoichiometry. Minimal variations in oxygen content can lead to vast changes in their properties. The addition of oxygen during synthesis may not be a precise enough knob for tuning the oxygen stoichiometry when the material has several stable and close oxidation states. We use sputtered $V_2O_3$ films as an example to show that rapid transfer of the sample away from the heating element after growth causes a temperature decrease (quenching) quick enough to freeze the correct oxygen stoichiometry in the sample. This procedure has allowed us to improve dramatically the $V_2O_3$ electronic properties without any adverse measurable effects on the structural properties. In this fashion, the metal–insulator transition resistance change was increased by two orders of magnitude, while the transition width was decreased by 20 K.

## Introduction

Oxides are one of the most widely studied systems in condensed matter physics and have important uses in modern technology [1–5]. They are used in the study of such diverse phenomena as exchange bias [6], high-temperature superconductivity [7], first-order phase transitions [8], or resistive switching [9]. In many of these cases, the observed properties depend delicately on the oxygen stoichiometry. For example, in the high-temperature superconducting $YBa_2Cu_3O_{7-\delta}$ (YBCO) a deviation of 0.5 in $\delta$ can completely suppress the superconducting phase and render the material an antiferromagnetic insulator [10–13]. Therefore, it is imperative to control precisely the oxygen stoichiometry to achieve the desired properties.

In thin-film deposition techniques like magnetron sputtering, evaporation or pulsed laser deposition, the control of oxygen stoichiometry is usually accomplished by growing the material in a partial oxygen atmosphere [14–17] or by a post-growth annealing [7, 18–23]. However, in certain cases it becomes very difficult to control the resulting level of oxidation after growth. This is usually caused by the high temperature needed to achieve good crystallinity, which facilitates oxygen stoichiometry changes during a relatively long cooldown. To avoid this issue, in certain cases an annealing followed by

Address correspondence to E-mail: jtrastoy@physics.ucsd.edu

https://doi.org/10.1007/s10853-018-2214-7

an extreme temperature decrease in liquid nitrogen [10, 24] or water [25] was used to freeze the correct oxygen content in YBCO. On the other hand, the insertion and extraction of oxygen through annealing can be utilized, as it has been proposed as a way to tune the properties and functionality of materials like SrCoO [26] or LaSrFeO [27].

Here, we focus on the case of vanadium sesquioxide ($V_2O_3$) [28–30]. This transition-metal oxide presents a first-order metal-to-insulator transition (MIT) at a temperature around 160 K, with a change in resistivity of several orders of magnitude. The MIT occurs concurrently with a rhombohedral to monoclinic structural phase transition (SPT) and a para- to antiferromagnetic phase transition. $V_2O_3$ has been studied intensely due to the long-standing debate over the microscopic origin of the phase transition [3, 31–34].

Very importantly, the physical properties of $V_2O_3$ depend very delicately on the oxygen stoichiometry. A slight variation in oxygen concentration changes the behaviour of properties like the electronic effective mass or heat capacity [35] and, eventually, the MIT and the antiferromagnetic state disappear, giving way to a metal with a spin density wave [36]. Moreover, several stable phases exist with diverse vanadium oxidation states that have significantly different electronic, structural and magnetic properties [37, 38]. For example, $VO_2$ presents a MIT around 340 K accompanied by a SPT, without a magnetic transition [30, 39]. Therefore, a careful tuning of the oxygen stoichiometry in $V_2O_3$ is a crucial aspect for its growth.

In this paper, we developed a simple way of freezing the correct oxygen stoichiometry achieved during growth of $V_2O_3$ thin films. In particular, we show that a marked improvement in the MIT properties is achieved by moving the sample away from the heating element right after the sputtering growth ("quenching"). Importantly, the significantly decreased MIT measured in unquenched samples grown with a partial oxygen atmosphere and annealed quenched samples underlined the sensitivity of the MIT to variations in the oxygen stoichiometry.

## Materials and methods

$V_2O_3$ thin films were grown on 7 × 12 mm *r*-cut sapphire substrates by RF magnetron sputtering deposition from a home-made $V_2O_3$ target. The target was fabricated by pressing stoichiometric $V_2O_3$ powder to 15 bar, followed by a 15.5-h bake at 1273 K in a 1.2% $H_2$, 98.8% Ar atmosphere. The base pressure of the sputtering system was $< 10^{-7}$ Torr. The samples were grown using a 7.7-sccm flow of ultrahigh-purity Ar (> 99.999%) atmosphere, resulting in an 8 mTorr Ar atmosphere, at a temperature of 1023 K, to achieve good crystallinity. Also, in order to study the sensitivity to the oxygen stoichiometry, some of the unquenched samples were grown adding oxygen. For this, we used two gas lines: one with pure Ar and the other with a 1.98%/98.02% $O_2$/Ar mixture, with a mass flow controller each to regulate the final proportion of Ar and $O_2$. This was done while maintaining constant the 8 mTorr sputtering pressure. The RF forward power during growth was 150 W with 0 W reflected, indicating good coupling of the power source to the gun. This resulted in a 2.5 Å/s deposition rate for a total thickness of 100 nm.

After the growth was finished, two different procedures were followed. For the unquenched samples, the temperature was ramped down using the heater at 12 K/min to room temperature in the same Ar atmosphere. For the quenched samples, right after the growth the sample was quickly transferred from the heater elements (halogen lamps) of the manipulator to the load lock. The procedure was done keeping the same 8 mTorr Ar environment. This achieved a rapid reduction in the sample temperature as the sample holder stopped glowing hot red after around 2–2.5 min. We had no means of directly measuring the temperature during quenching, but a rough estimate can be calculated. Assuming that the temperature at which the glowing stops (known as the "Draper point" [40]) in our Inconel substrate holder is similar to other metals, 798 K [40], the cooling rate was on the order of 100 K/min. This was almost ten times faster than in the unquenched sample. The cooldown in the load lock after the Draper point is estimated to be around 40 K/min, based on the time it takes for the substrate holder to reach 325 K. This rate is much faster than for the unquenched sample because its 12 K/min cooling rate is achieved thanks to the heater, which continues to supply heat after the growth.

For one of the quenched samples, a hotplate at 393 K was used to anneal the sample in air in order to test its sensitivity to oxygen stoichiometry variations at low temperatures.

The samples were characterized in two ways. The temperature-dependent four-probe electrical transport was performed in a Quantum Design Dynacool PPMS using a Keithley 6221 current source and a Keithley 2182A nanovoltmeter behind two Keithley 6517A electrometers acting as a buffer. This allows us to measure the highest resistances accurately. The temperature was ramped at 2 K/min in all cases. In addition, X-ray reflectivity (XRR) and diffraction (XRD) characterization was done in a Rigaku Smartlab diffractometer using a Ge (220) monochromator for Cu $K_{\alpha 1}$ = 0.154 nm wavelength in the Bragg–Brentano configuration [see inset Fig. 1a].

## Results

Figure 1a, b shows the XRR and XRD patterns, respectively, of quenched (red line) and unquenched (black line) $V_2O_3$ samples both grown in a pure Ar atmosphere. The oscillations in Fig. 1a have a period of $\Delta 2\theta \sim 0.08°$ in both cases, which corresponds to a thickness of $\sim$ 110 nm. The roughness was determined to be $\sim$ 2 nm for both samples through XRR refinement with Motofit [41] (see Supplementary Information for fitting curves and parameters). In the diffraction curves shown in Fig. 1b, there are two peaks corresponding to the r-cut sapphire substrate at $2\theta = 25.6°$ (012) and 52.5° (024), and three $V_2O_3$ peaks of the (012) family of planes at 24.3°, 49.8° and 78.2°. The sapphire peaks have a lower intensity due to the misalignment between the $V_2O_3$ (012) plane and the substrate's *r*-plane. The inset of Fig. 1b shows the rocking curve around the (012) peak for each sample, yielding very similar results with a full width at half maximum of 0.638°. Reciprocal space maps for the quenched and unquenched samples [Fig. 1c left and right panels, respectively] aligned to the $V_2O_3$ (104) peak show that all peaks correspond to a single orientation of the rhombohedral crystal structure.

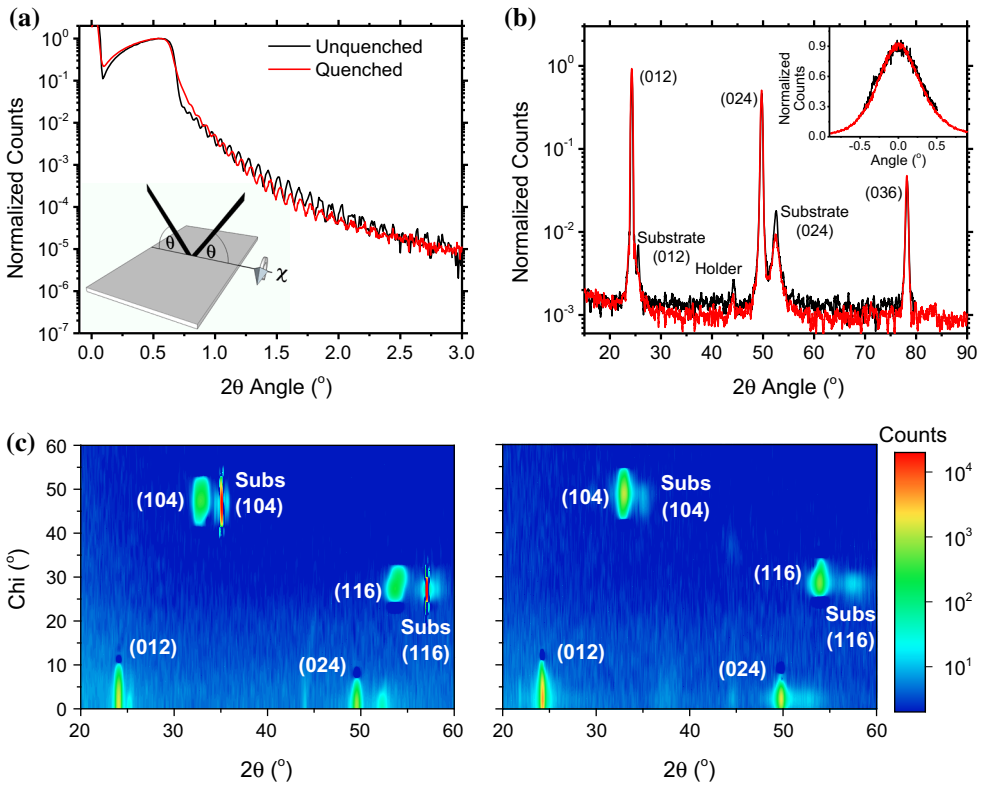


**Figure 1** X-ray measurements of $V_2O_3$ thin films grown in a pure Ar atmosphere in **a** reflectivity (normalized to the critical edge intensity), **b** out-of-plane diffraction (normalized to the $V_2O_3$ (012) peak), and **c** reciprocal space mapping. The inset in **a** shows the Bragg–Brentano measurement configuration. The black and red lines in **a**, **b** correspond to unquenched and quenched samples, respectively. The inset in **b** shows the rocking curve around the (012) peak for both samples. The full width at half maximum is 0.638°. The left panel in **c** corresponds to a quenched sample grown in pure Ar. The right panel corresponds to an unquenched sample grown in the same conditions. In both cases, an epitaxial growth along the (012) direction is obtained.

This confirms that our films grow epitaxially along the (012) direction with lattice constants $a$ = 0.494 nm and $c$ = 1.403 nm. The value for $a$ is 0.27% smaller than in bulk $V_2O_3$ ($a$ = 0.495 nm) due to the compressive strain from the sapphire substrate ($a$ = 0.476 nm), while $c$ is 0.22% larger than in bulk $V_2O_3$ ($c$ = 1.400 nm).

Figure 2 shows the resistivity ρ normalized by the metallic state resistivity $\rho_m$ as a function of temperature for a quenched $V_2O_3$ (red line) and an unquenched film (black line) grown in a pure Ar atmosphere. The metal–insulator transition (MIT) causes a several-order-of-magnitude change in the resistivity. The temperature at which the transition begins is very similar for both samples, around 175 K (bottom arrows). On the other hand, there is a clear difference in both the width and the magnitude of the transition. We define the width as the temperature difference between the beginning and the end of the transition; the magnitude is defined as the ratio $\rho_i/\rho_m$, the resistivities at the end (top arrow) and beginning (bottom arrow) of the transition, respectively. The magnitude for the quenched sample is about two orders of magnitude higher than that of the unquenched film. Also, the transition in the quenched sample is extremely sharp: its width is 20 K lower than in the unquenched sample. The hysteresis width (the temperature difference between the cooling and heating branches) remains constant during the central part of the MIT. However, the curve of the unquenched sample closes at much lower temperatures.

Figure 3 shows a comparison of a quenched sample before (red) and after (blue) annealing in air at 393 K for 5 min. A significant degradation of the MIT in the annealed sample is observed. The blue curve has a much smaller magnitude and is wider, similar to the unquenched samples (black curve in Fig. 2). There are even signs of severe inhomogeneity in the sample with a deformed hysteresis loop.

We also tried adding $O_2$ during growth to investigate whether increasing the oxygen stoichiometry could improve the transition in unquenched samples. For this, the sputtering was performed adding a 1.98%/98.02% mixture of $O_2$ and Ar to the previous Ar flow as described in the methods section. We were limited by the fact that the mass flow controllers cannot regulate the mixture flow below 1 sccm. This allowed us to mix a minimum of 0.28% $O_2$ in the chamber during growth while preserving the same growth total pressure. This gives an oxygen partial pressure of $2 \times 10^{-5}$ Torr, which is at least two orders of magnitude higher than the ones found in

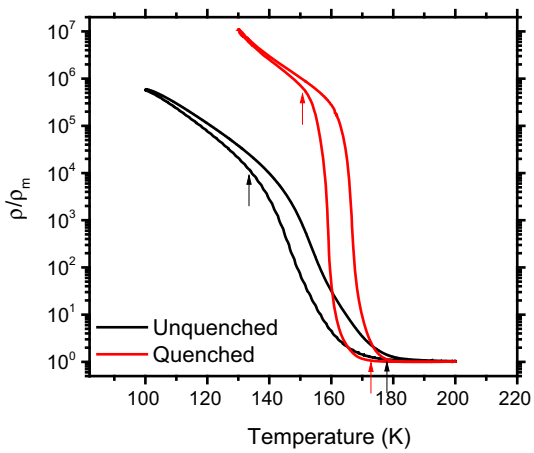


**Fig. 2** Normalized resistivity as a function of temperature for both the quenched (red line) and unquenched (black line) samples grown in a pure Ar atmosphere. The normalization has been done to the minimum resistivity, $\rho_m$, in the metallic phase (quenched $9.0 \times 10^{-6}$ Ωm, unquenched $6.4 \times 10^{-6}$ Ωm). Both the magnitude and width of the metal–insulator transition are improved when the films are quenched. The black and red arrows mark the beginning and end of the MIT for the unquenched and quenched samples, respectively.

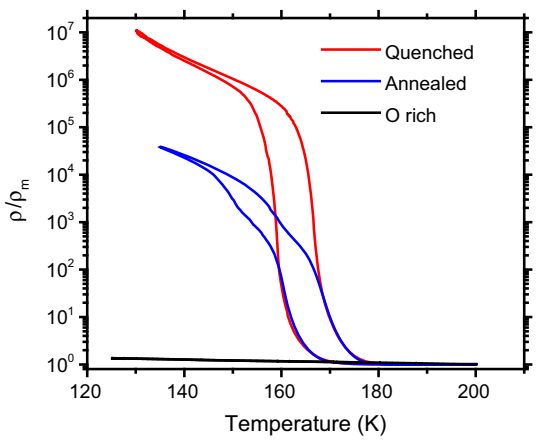


**Fig. 3** Normalized resistivity as a function of temperature for a quenched sample (red line) grown in Ar atmosphere, the same sample after annealing at 393 K in air for 5 min (blue line), and an unquenched sample grown with an atmosphere of 0.28% oxygen (black line). The normalization has been done to the lowest resistivity in the metallic phase, $9.0 \times 10^{-6}$ Ωm, for the first two, and to the resistivity at 200 K, $2.1 \times 10^{-5}$ Ωm, for the O-rich sample. The deformation and dispersion of the MIT towards lower temperatures in the annealed sample illustrates the deterioration of $V_2O_3$. No transition is observed for the O-rich sample.

the literature [14, 42]. The addition of $O_2$ suppressed the transition completely and rendered the film semiconducting (black curve of Fig. 3). The relatively low resistivity ($2 \times 10^{-5}$ Ωm) of this film suggests that an O-rich $V_2O_3$ film was obtained, rather than a completely different vanadium oxide phase like $V_3O_5$, $V_4O_7$, or $VO_2$, which are insulating and much more resistive in the measured temperature range [37].

## Discussion

The comparison between quenched and unquenched samples (Fig. 2) shows that the electronic properties improved markedly when the temperature is rapidly decreased after growth: the MIT is sharper and displays a two-order-of-magnitude higher resistivity change.

The observed results could be explained in two ways: (1) the quenched samples have an improved crystalline structure; or (2) the oxygen stoichiometry in the quenched samples is closer to the optimal value. In principle, both would lead to an enhanced MIT. However, the first possibility does not match our results in X-ray characterization results. Fig. 1b, c shows crystallinity in the quenched sample is not significantly better. Thus, the enhanced transport does not correlate with an improvement in the structure. This leaves only option 2, which leads to a very important conclusion: the time that the sample spends at high temperature after growth results in a reduction in the oxygen content, changing it away from the optimal stoichiometry. This, in turn, results in adverse effects on the MIT magnitude and width. We must also address the question of homogeneity in the films. Given the fact that the surface is the most exposed part, it is likely that an oxygen gradient exists, where the surface has the lowest concentration. A further cause of inhomogeneities is that during cooling down the part of the film closest to the substrate is at a higher temperature than the surface. Shortening this time as much as possible effectively limits this effect. This relationship between homogeneities and the difference in width observed in the MIT in Figs. 2 and 3 is indicative of the distribution in the transition temperatures of each film. For the unquenched sample grown in pure Ar and the annealed quenched sample, the width is much larger, possibly due to a big dispersion in the transition temperature of the different domains. The more homogeneous quenched sample would have a smaller dispersion and, thus, a significantly smaller width.

It is important to note that this improvement in the material properties of $V_2O_3$ produces no significant changes in the structure. One may expect that quenching would freeze structural defects in the material, thus producing a more disordered film. However, that is not what we observe. X-ray diffraction measurements show that quenched and unquenched films have the same (012) epitaxial structure, with similar linewidths and well-defined orientations. This could be due to the fact that we are using a rather "slow" form of quenching when compared to liquid-cooled techniques.

The conclusions presented above are also supported by the observed sensitivity to oxygen content of $V_2O_3$. Significant degradation of the metal–insulator transition can be observed when heating up the samples above 393 K in air (Fig. 3). Also, the addition of 0.28% $O_2$ during growth makes the transition disappear (Fig. 3).

This sensitivity to the oxygen stoichiometry is common to all oxides and is an important concern for applications based on these materials [3, 43–45]. The rapid transfer out of the chamber of the sample after growth was proven to be an effective tool for preserving the optimal oxygen stoichiometry. Note that, in this case, our technique was the only method that worked, since adding oxygen during growth produced a complete suppression of the MIT. This quenching technique is much simpler than the extremely rapid quenching with liquids and does not involve the need of quartz sheaths [25] or complicated setups and mechanisms to drop the sample in the liquid [10]. Our method can also be applied to any deposition technique for oxide growth at high temperature. After growth is complete, quenching will prevent loss of oxygen during cooling and will likely result in a more homogeneous oxygen stoichiometry across the film.

## Conclusion

In summary, we have demonstrated that fast temperature quenching after growth can be achieved by quickly transferring the sample out of the deposition chamber. This technique applied to oxide materials deposition is an effective tool to freeze in the correct

oxygen stoichiometry achieved during growth, and allows for a more precise optimization of the material properties. In our case, quenching $V_2O_3$ thin films after high-temperature RF sputtering growth leads to a marked improvement in the MIT. We showed a two-order-of-magnitude higher resistivity change and a 20-K transition width decrease, without any noticeable structural changes. Our work shows that further high-precision techniques which allow the measurement and characterization of oxygen stoichiometry in novel materials are needed if oxides are to be used in the next generation of applications.

## Acknowledgements

Work supported by the Vannevar Bush Faculty Fellowship program sponsored by the Basic Research Office of the Assistant Secretary of Defense for Research and Engineering and funded by the Office of Naval Research through Grant N00014-15-1-2848. J. Trastoy and J. del Valle thank the Fundación Ramón Areces for a postdoctoral fellowship.

## Compliance with ethical standards

**Conflict of interest** The authors declare no conflict of interests.

**Electronic supplementary material:** The online version of this article (https://doi.org/10.1007/s10853-018-2214-7) contains supplementary material, which is available to authorized users.

## References

[1] Simon P, Gogotsi Y (2008) Materials for electrochemical capacitors. Nat Mater 7:845–854

[2] Catalan G, Scott JF (2009) Physics and applications of bismuth ferrite. Adv Mater 21:2463–2485

[3] Yang Z, Ko C, Ramanathan S (2011) Oxide electronics utilizing ultrafast metal-insulator transitions. Annu Rev Mater Res 41:337–367

[4] Zhou You, Ramanathan S (2015) Mott memory and neuromorphic devices. Proc IEEE 103:1289–1310

[5] Lorenz M, Ramachandra Rao MS, Venkatesan T et al (2016) The 2016 oxide electronic materials and oxide interfaces roadmap. J Phys D Appl Phys 49:1–53

[6] Nogués J, Schuller IK (1999) Exchange bias. J Magn Magn Mater 192:203–232

[7] Bednorz JG, Müller KA (1986) Possible high Tc superconductivity in the Ba–La–Cu–O system. Z Phys B Condens Matter 64:189–193

[8] Imada M, Fujimori A, Tokura Y (1998) Metal-insulator transitions. Rev Mod Phys 70:1039–1263

[9] Sawa A (2008) Resistive switching in transition metal oxides. Mater Today 11:28–36

[10] Jorgensen JD, Veal BW, Kwok WK et al (1987) Structural and superconducting properties of orthorhombic and tetragonal $YBa_2Cu_3O_{7-x}$: the effect of oxygen stoichiometry and ordering on superconductivity. Phys Rev B 36:5731–5734

[11] Tranquada JM, Moudden AH, Goldman AI et al (1988) Antiferromagnetism in $YBa_2Cu_3O_{6+x}$. Phys Rev B 38:2477–2485

[12] Schuller IK, Jorgensen JD (1989) Structure of high Tc oxide superconductors. MRS Bull 14:27–30

[13] Jorgensen JD, Veal BW, Paulikas AP et al (1990) Structural properties of oxygen-deficient $YBa_2Cu_3O_{7-d}$. Phys Rev B 41:1863–1877

[14] Biener J, Bäumer M, Madix RJ et al (1999) A synchrotron study of the growth of vanadium oxide on $Al_2O_3$(0001). Surf Sci 441:1–9

[15] Sharoni A, Ramírez JG, Schuller IK (2008) Multiple avalanches across the metal-insulator transition of vanadium oxide nanoscaled junctions. Phys Rev Lett 101:1–4

[16] Dillemans L, Lieten RR, Menghini M et al (2012) Correlation between strain and the metal-insulator transition in epitaxial $V_2O_3$ thin films grown by Molecular Beam Epitaxy. Thin Solid Films 520:4730–4733

[17] Masina BN, Lafane S, Wu L et al (2015) Optimizing the synthesis of vanadium–oxygen nanostructures by plasma plume dynamics using optical imaging. Opt Eng 54:1–8

[18] Yun SJ, Lim JW, Noh JS et al (2009) Vanadium dioxide and vanadium sesquioxide thin films fabricated on (0001) or (1010) $Al_2O_3$ by reactive RF-magnetron sputter deposition and subsequent annealing processes. Jpn J Appl Phys 48:1–4

[19] Billik P, Cigáň A, Čaplovičová M et al (2013) $V_2O_3$ nanocrystals prepared by mechanochemical–thermal reduction and their magnetic properties. Mater Lett 110:24–26

[20] Lee S, Meyer TL, Park S et al (2014) Growth control of the oxidation state in vanadium oxide thin films. Appl Phys Lett 105:1–4

[21] Van Bilzen B, Homm P, Dillemans L et al (2015) Production of $VO_2$ thin films through post-deposition annealing of $V_2O_3$ and $VO_x$ films. Thin Solid Films 591:143–148

[22] Xu HY, Huang YH, Liu S et al (2016) Effects of annealing ambient on oxygen vacancies and phase transition temperature of $VO_2$ thin films. RSC Adv 6:79383–79388

[23] Zhan Y, Xiao X, Lu Y, et al (2017) High performance $VO_2$ thin films fabricated by room-temperature reactive magnetron sputtering and rapid thermal annealing. In: Qiu M, Gu M, Yuan X, Zhou Z (eds) AOPC 2017 Optoelectron. Micro/nano-optics. SPIE, p 30

[24] Farneth WE, Bordia RK, McCarron EM et al (1988) Influence of oxygen stoichiometry on the structure and superconducting transition temperature of $YBa_2Cu_3O_x$. Solid State Commun 66:953–959

[25] Xie XM, Chen TG, Wu ZL (1989) Oxygen diffusion in the superconducting oxide $YBa_2Cu_3O_{7-x}$. Phys Rev B 40:4549–4556

[26] Choi WS, Jeen H, Lee JH et al (2013) Reversal of the lattice structure in $SrCoO_x$ epitaxial thin films studied by real-time optical spectroscopy and first-principles calculations. Phys Rev Lett 111:1–5

[27] Islam MA, Xie Y, Scafetta MD et al (2015) Raman scattering in $La_{1-x}Sr_xFeO_{3-\delta}$ thin films: annealing-induced reduction and phase transformation. J Phys Condens Matter 27:1–7

[28] Morin FJ (1959) Oxides which show a metal-to-insulator transition at the Neel temperature. Phys Rev Lett 3:34–36

[29] McWhan DB, Remeika JP (1970) Metal-insulator transition in $(V_{1-x}Cr_x)_2O_3$. Phys Rev B 2:3734–3750

[30] Shin S, Suga S, Taniguchi M et al (1990) Vacuum-ultraviolet reflectance and photoemission study of the metal-insulator phase transitions in $VO_2$, $V_6O_{13}$, and $V_2O_3$. Phys Rev B 41:4993–5009

[31] Rozenberg MJ, Kotliar G, Kajueter H et al (1995) Optical conductivity in Mott-Hubbard systems. Phys Rev Lett 75:105–108

[32] Held K, Keller G, Eyert V et al (2001) Mott-Hubbard metal-insulator transition in paramagnetic $V_2O_3$: an LDA + DMFT(QMC) study. Phys Rev Lett 86:5345–5348

[33] Rodolakis F, Hansmann P, Rueff JP et al (2010) Inequivalent routes across the mott transition in $V_2O_3$ explored by X-ray absorption. Phys Rev Lett 104:1–4

[34] Ramirez JG, Saerbeck T, Wang S et al (2015) Effect of disorder on the metal-insulator transition of vanadium oxides: local versus global effects. Phys Rev B 91:1–5

[35] Carter SA, Rosenbaum TF, Metcalf P et al (1993) Mass enhancement and magnetic order at the Mott-Hubbard transition. Phys Rev B 48:16841–16844

[36] Bao W, Broholm C, Carter SA et al (1993) Incommensurate spin density wave in metallic $V_{2-y}O_3$. Phys Rev Lett 71:766–769

[37] Kachi S, Kosuge K, Okinaka H (1973) Metal-insulator transition in $V_nO_{2n-1}$. J Solid State Chem 6:258–270

[38] Griffiths CH, Eastwood HK (1974) Influence of stoichiometry on the metal-semiconductor transition in vanadium dioxide. J Appl Phys 45:2201–2206

[39] Marezio M, McWhan DB, Remeika JP, Dernier PD (1972) Structural aspects of the metal-insulator transitions in Cr-doped $VO_2$. Phys Rev B 5:2541–2551

[40] Draper JW (1847) On the production of light by heat. Philos Mag J Sci 30:345–359

[41] Nelson A (2006) Co-refinement of multiple-contrast neutron/X-ray reflectivity data using *MOTOFIT*. J Appl Crystallogr 39:273–276

[42] Sun G, Cao X, Long S et al (2017) Optical and electrical performance of thermochromic $V_2O_3$ thin film fabricated by magnetron sputtering. Appl Phys Lett 111:1–5

[43] Jorgensen JD, Beno MA, Hinks DG et al (1987) Oxygen ordering and the orthorhombic-to-tetragonal phase transition in $YBa_2Cu_3O_{7-x}$. Phys Rev B 36:3608–3616

[44] Wuyts B, Vanacken J, Locquet J-P, et al (1990) Oxygen evolution in high-Tc superconductors. In: Proceedings of the NATO A.S.I. high temperature superconductivity. Kluwer, Dordrecht, Netherlands, pp 307–318

[45] Wang ZL (2004) Zinc oxide nanostructures: growth, properties and applications. J Phys Condens Matter 16:R829–R858